INTERNATIONAL JOURNAL FOR NUMERICAL METHODS IN ENGINEERING
Int. J. Numer. Meth. Engng 2001; **50**:395–418

An adaptive finite element approach for frictionless contact problems

Gustavo C. Buscaglia[1,‡], Ricardo Durán[2,§], Eduardo A. Fancello[3,¶], Raúl A. Feijóo[4,*,†] and Claudio Padra[1]

[1] *Instituto Balseiro, Centro Atómico Bariloche (CAB), 8400 Bariloche, Argentina*
[2] *Departamento de Matemáticas, Universidad de Buenos Aires, Ciudad Universitaria, Pabellón 1, 1428 Buenos Aires, Argentina*
[3] *Departamento de Mecânica, Universidade Federal de Santa Catarina, Brazil*
[4] *Laboratório Nacional de Computação Científica (LNCC/CNPq), Av. Getúlio Vargas 333, 25651-070 Petrópolis, RJ, Brazil*

SUMMARY

The derivation of an *a posteriori* error estimator for frictionless contact problems under the hypotheses of linear elastic behaviour and infinitesimal deformation is presented. The approximated solution of this problem is obtained by using the finite element method. A penalization or augmented-Lagrangian technique is used to deal with the unilateral boundary condition over the contact boundary. An *a posteriori* error estimator suitable for adaptive mesh refinement in this problem is proposed, together with its mathematical justification. Up to the present time, this mathematical proof is restricted to the penalization approach. Several numerical results are reported in order to corroborate the applicability of this estimator and to compare it with other *a posteriori* error estimators. Copyright © 2001 John Wiley & Sons, Ltd.

KEY WORDS: error estimator; adaptive analysis; frictionless contact problems; finite element method

1. INTRODUCTION

Computationally efficient adaptive procedures for the numerical solution of variational inequalities of elliptic type, which arise e.g. in frictionless elastic contact problems, have received special attention over the last years [1, 2]. This is because powerful mathematical programming algorithms

*Correspondence to: Raúl A. Feijóo, Depto de Mecânica Computacional, LNCC/CNPq, Av. Getúlio Vargas 333, 25651-070 Petrópolis, RJ, Brazil
†E-mail: feij@lncc.br
‡E-mail: gustavo@cab.cnea.gov.ar, padra@cab.cnea.gov.ar
§E-mail: rduran@mate.dm.edu.ar
¶E-mail: fancello@emc.ufsc.br

Contract/grant sponsor: Conselho Nacional de Desenvolvimento Científico e Tecnologico, Brazil
Contract/grant sponsor: Consejo Nacional de Investigaciones Científicas y Técnicas, Argentina
Contract/grant sponsor: Fundação de Amparo à Pesquisa do Estado de Rio de Janerio

Received 6 October 1999
Revised 10 January 2000

have become available, together with efficient numerical methods (such as finite elements [3]) and their integration with solid modelling, visualization of engineering data and automatic mesh generation.

In any adaptive procedure, *a posteriori* error estimators play an important role in the process of assessing the accuracy of the approximate solution. Based on the information given by these estimators, it is possible to decide whether the adaptive process must be stopped or, if this is not the case, where and how mesh refinement might be performed more efficiently (see Reference [4] and the references therein).

In the linear case, several approaches are available to define error estimators for different problems using the residual equation (see, for example, References [5–9]). To extend these techniques to variational inequalities, the main difficulty is that the error is not orthogonal to the set of approximate functions. This feature yields terms in the error equation that depend on the exact solution and cannot be neglected.

Local *a posteriori* error estimators for variational inequalities have been proposed by Ainsworth *et al*. [1] and applied to the obstacle problem. Following a different approach, Johnson also reports in Reference [2] an adaptive finite element method for the same problem.

We have used Johnson's ideas to derive an *a posteriori* error estimator for the frictionless contact problem, which differs from the obstacle problem in that an inequality constraint must hold at the boundary of the domain instead of in its interior. This error estimator is then used in adaptive finite element solution of test problems to assess the reliability and computational efficiency of this estimator.

The presentation is organized as follows: In Section 2, the primal formulation of the mathematical model and its optimality conditions are briefly reviewed. The penalization technique and finite element approximation are also included. Based on the penalized approach, an *a posteriori* error estimator is proposed in Section 3. It is also proved in this section that this estimator provides an upper bound for the discretization error. Numerical evidence that the optimal order of convergence is obtained with an adaptive procedure based on this estimator and its comparison with other *a posteriori* error estimators in the literature are provided through several numerical experiments in Section 4.

2. CONTACT PROBLEM

Let us consider a bounded region Ω in $\mathbf{R}^2$ with boundary $\Gamma = \Gamma_c \cup \Gamma_f \cup \Gamma_u$, occupied by an elastic homogeneous body $\mathscr{B}$ submitted to surface tractions f over Γ_f and body forces b over Ω. Displacements u take a prescribed value in Γ_u (equal to zero for simplicity) and the unilateral contact between $\mathscr{B}$ and a rigid body (foundation) $\mathscr{F}$ potentially takes place over Γ_c.

Let $\mathbf{T}$ be the stress-tensor field, obtained as the derivative of a potential function W with respect to the symmetric gradient of displacements

$$\mathbf{T}(u) = \frac{\partial W}{\partial \nabla u^s}, \quad W(u) = \frac{1}{2}\mathbf{C}\nabla u^s \cdot \nabla u^s \tag{1}$$

where $\mathbf{C}$ is the fourth-order elastic tensor satisfying the usual assumptions of symmetry and strong ellipticity.

Given a local orthonormal system (τ, n) at each point $x \in \Gamma_c$ (tangential and outward normal unit vectors, respectively), we call $\sigma_n = \mathbf{T}n \cdot n$ and $\sigma_\tau = \mathbf{T}n \cdot \tau$ the normal and tangential components of

the force exerted by the foundation $\mathscr{F}$ on $\mathscr{B}$ across Γ_c. We also assume that the gap s between Γ_c and $\mathscr{F}$ in the normal direction n is zero.

We define

$$\mathbf{V} = \{v \in (H^1(\Omega))^2 : \ v = 0 \text{ on } \Gamma_u\}$$

$$K = \{v \in \mathbf{V} : \ g(v) \equiv v \cdot n \leqslant 0 \text{ on } \Gamma_c\}$$

where K is the convex set of admissible displacements, i.e. compatible with the kinematical constraints over Γ_c and Γ_u.

Given the bilinear form $a(\cdot,\cdot)$ and the linear form $l(\cdot)$,

$$a(u,v) = \int_\Omega \mathbf{T}(u) \cdot \nabla v^{\mathrm{s}} \, \mathrm{d}\Omega, \quad l(v) = \int_\Omega b \cdot v \, \mathrm{d}\Omega + \int_{\Gamma_f} f \cdot v \, \mathrm{d}\Gamma \tag{2}$$

the solution of the Signorini problem without friction is given by the following minimization problem: find $u \in K$ such that

$$u = \arg \inf_{v \in K} J(v), \quad J(v) = \tfrac{1}{2} a(v,v) - l(v) \tag{3}$$

or, equivalently

$$u = \arg \inf_{v \in \mathbf{V}} Ł(v), \quad Ł(v) = J(v) + I_K(v) \tag{4}$$

where I_K is the indicator function of the convex set K.

As it is well known, this constrained optimization problem is formally equivalent to the saddle point (inf–sup) problem: find $u \in \mathbf{V}$ and $\lambda \in \Lambda^+$ such that

$$(u,\lambda) = \arg \inf_{v \in \mathbf{V}} \sup_{\lambda^* \in \Lambda^+} \{J(v) + \langle \lambda^*, g(v) \rangle\} \tag{5}$$

where the admissible convex cone Λ^+ for the Lagrange multipliers λ is defined by

$$\Lambda^+ = \{\lambda^* \in H^{-1/2}(\Gamma_c); \lambda^* \geqslant 0 \text{ a.e on } \Gamma_c\}$$

and $\langle \cdot,\cdot \rangle$ denotes the duality pairing between $H^{-1/2}(\Gamma_c)$ and $H^{1/2}(\Gamma_c)$. From the mechanical point of view, λ represents the reaction (dual force) associated with the unilateral kinematical restriction $g(u) \equiv u \cdot n \leqslant 0$ imposed on Γ_c.

Conditions for existence and uniqueness of the solution for all these abstract problems are thoroughly analysed in References [10–12]. The solution $u \in K$ of (3) is characterized by the following variational inequality problem: find $u \in K$ such that

$$a(u, v-u) \geqslant l(v-u), \quad \forall v \in K \tag{6}$$

Moreover, this solution is also solution of the saddle point problem (5) which is characterized by: find $(u,\lambda) \in \mathbf{V} \times \Lambda^+$ such that

$$\begin{aligned} &a(u,v) + \langle \lambda, v \rangle = l(v), \quad \forall v \in \mathbf{V} \\ &\langle \lambda^* - \lambda, g(u) \rangle \leqslant 0, \quad \forall \lambda^* \in \Lambda^+ \end{aligned} \tag{7}$$

Another possible way to solve the primal problem (3) is to use penalty techniques. In this case, the indicator function I_K is approximated by a penalty function $P_\varepsilon = \varepsilon^{-1}P$, $\varepsilon > 0$, satisfying the following conditions [12, 13]:

$$P : \mathbf{V} \to \Re \text{ is weakly lower semicontinuous}$$

$$P(v) \geqslant 0,\ P(v) = 0 \text{ if and only if } v \in K$$

$$P \text{ is Gateaux differentiable on } \mathbf{V}$$

For the contact problem without friction, a natural choice for P_ε satisfying the above properties is given by

$$P_\varepsilon(v) = \int_{\Gamma_c} \frac{1}{2\varepsilon}[g(v)^+]^2 \, \mathrm{d}\Gamma_c = \left\langle \frac{1}{2\varepsilon}[g(v)]^+, [g(v)]^+ \right\rangle$$

where $[\cdot]^+$ is the positive part of $[\cdot]$. In this approach, the solution u_ε given by the penalty method is now characterized by the unconstrained minimization problem: find $u_\varepsilon \in \mathbf{V}$ such that

$$u_\varepsilon = \arg \inf_{v \in \mathbf{V}} \{J_\varepsilon(v) = J(v) + P_\varepsilon(v)\} \tag{8}$$

Moreover, due to the properties of J_ε, u_ε is also given by the following non-linear variational equation: find $u_\varepsilon \in \mathbf{V}$ such that

$$a(u_\varepsilon, v) + \left\langle \frac{1}{\varepsilon}[g(u_\varepsilon)]^+, g(v) \right\rangle = l(v), \quad \forall v \in \mathbf{V} \tag{9}$$

As was shown by Kikuchi and Oden [12], the sequence $(u_\varepsilon, j((1/\varepsilon)[g(u)]^+))$ strongly converges to (u, λ) in $\mathbf{V} \times H^{-1/2}(\Gamma_c)$ as $\varepsilon \to 0$. Above, j is the Riesz map from $H^{1/2}(\Gamma_c)$ to $H^{-1/2}(\Gamma_c)$.

In order to obtain approximate solutions, a finite-dimensional counterpart of all these variational problems must be built using, for instance, finite elements. Actually, taking linear triangular finite elements and denoting by I the set of indices i such that $x_i \in \Gamma_c$ is a nodal point, the convex set K can be approximated by

$$K_h = \{v_h \in \mathbf{V}_h : g(v_h(x_i)) \leqslant 0,\ i \in I\}$$

Then, the approximated solution $u_h \in K_h$ of (3) is given by

$$u_h = \arg \inf_{v_h \in K_h} J(v_h) \tag{10}$$

where $\mathbf{V}_h$ is a finite-dimensional subspace of $\mathbf{V}$. Thus, u_h is the solution of the minimization of a quadratic functional with inequality constraints. The solution could be obtained by several mathematical programming algorithms. The LEMKE method, for example, finds the solution u_h in a finite number of steps. Another possibility is to use a mathematical programming technique like the one proposed by Herskovits [14], also applied by Fancello and Feijóo in an optimal contact shape design context [15] (see also References [16, 17]).

On the other hand, the penalty approach consists of: find $u_{\varepsilon h} \in \mathbf{V}_h$ such that

$$u_{\varepsilon h} = \arg \inf_{v_h \in \mathbf{V}_h} \{J_\varepsilon(v_h) = J(v_h) + P_\varepsilon(v_h)\} \tag{11}$$

which means that $u_{\varepsilon h}$ is the solution of the minimization of a functional defined on the finite-dimensional subspace $\mathbf{V}_h$ of $\mathbf{V}$. This solution is also given by the following non-linear variational equation which is the finite-dimensional counterpart of (9): find $u_{\varepsilon h} \in \mathbf{V}_h$ such that

$$a(u_{\varepsilon h}, v_h) + \left\langle \frac{1}{\varepsilon}[g(u_{\varepsilon h})]^+, g(v_h) \right\rangle = l(v_h), \quad \forall v_h \in \mathbf{V}_h \tag{12}$$

However, it is well known that penalty formulations have the drawback that numerical instabilities arise for small values of ε. In order to overcome this difficulty, several procedures were proposed. Among them, the augmented-Lagrangian technique (see Reference [18]), which provides the approximate solution u_h of (10) as the limit of a sequence of penalized problems. The specific augmented-Lagrangian algorithm we use is described in the appendix (see also References [17, 15, 19]).

In the next section we prove that our *a posteriori* error estimator, based on the penalized formulation (12), yields an upper bound for the error in the approximate solution. In other words, we will prove that for a given ε

$$\|u_\varepsilon - u_{\varepsilon h}\| \leqslant C\eta^*$$

where $\|\cdot\|$ is an appropriate norm specified in the next section, C is a constant independent of h and ε, and η^* our *a posteriori* error estimator.

3. *A POSTERIORI* ERROR ESTIMATOR FOR THE CONTACT PROBLEM

Let us assume that we have a family $\mathscr{T}_h$ of regular triangulations of the domain Ω such that any two triangles in $\mathscr{T}_h$ share at most a vertex or an edge. Given an interior edge ℓ we choose an arbitrary normal direction n_ℓ and denote by T_{in} and T_{out} the two triangles sharing this edge with n_ℓ pointing outward T_{in}. If $n_\ell = (n_1, n_2)$, we define the tangent $\tau_\ell = (-n_2, n_1)$. When $\ell \in \Gamma$, n_ℓ is the outward normal. Then, we denote by

$$[\![\mathbf{T}(u_h)n]\!]_\ell = [\mathbf{T}(u_h)|_{\text{out}} n_\ell] - [\mathbf{T}(u_h)|_{\text{in}} n_\ell]$$

the jump of $\mathbf{T}(u_h)n_\ell$ across ℓ in the direction n_ℓ.

Let $\mathscr{E}_{\text{I}}$ be the set of interior edges of $\mathscr{T}_h$ and for an element T, let E_T be the set of edges of T. Moreover, for a given $T \in \mathscr{T}_h$, we denote by $\tilde{T}$ the domain defined by T and all elements in $\mathscr{T}_h$ sharing a common vertex with T. Finally, we denote by $|T|$ and $|\ell|$ the area of the element T and the length of the edge ℓ.

In this section, we present an *a posteriori* error estimator suitable for automatic mesh refinement in the numerical evaluation of the contact problem by finite elements. As stated above, the initial gap s between Γ_c and the rigid foundation $\mathscr{F}$ is assumed to be zero in order to simplify our presentation. Also, the standard notation for Sobolev spaces, norms and seminorms will be used. In particular, the seminorm in the space $(H^1(\Omega))^2$ will be denoted by $|v|_{1,\Omega}$. Moreover, the bilinear form $a(\cdot,\cdot) : \mathbf{V} \times \mathbf{V} \to \mathbf{R}$ satisfies the following properties:

$$|a(u,v)| \leqslant M|u|_{1,\Omega}|v|_{1,\Omega}, \quad \forall u, v \in \mathbf{V}$$

$$a(u,u) \geqslant \alpha|u|^2_{1,\Omega}, \quad \forall u \in \mathbf{V}$$

Let us consider the penalized formulation defined in (9)

$$a(u_\varepsilon, v) + \langle \varepsilon^{-1}[g(u_\varepsilon)]^+, g(v)\rangle = l(v), \quad \forall v \in \mathbf{V} \tag{13}$$

Moreover, the approximate finite element solution of (13) verifies (12)

$$a(u_{\varepsilon h}, v_h) + \langle \varepsilon^{-1}[g(u_{\varepsilon h})]^+, g(v_h)\rangle = l(v_h), \quad \forall v_h \in \mathbf{V}_h \tag{14}$$

Let us also introduce the non-linear form

$$A(u, v) = a(u, v) + \langle \varepsilon^{-1}[g(u)]^+, g(v)\rangle$$

From the above definitions and notations, the following lemma can be established.

Lemma 1. There exists a positive constant C such that

$$|u - v|^2_{1,\Omega} + \|\varepsilon^{-1/2}([g(u)]^+ - [g(v)]^+)\|^2_{0,\Gamma_c} \leqslant C(A(u, u - v) - A(v, u - v)), \quad \forall u, v \in \mathbf{V}$$

Proof. From the coercivity property of the bilinear form a it follows that

$$\alpha|u - v|^2_{1,\Omega} + \|\varepsilon^{-1/2}([g(u)]^+ - [g(v)]^+)\|^2_{0,\Gamma_c}$$

$$\leqslant a(u - v, u - v) + \int_{\Gamma_c} \varepsilon^{-1}([g(u)]^+ - [g(v)]^+)([g(u)]^+ - [g(v)]^+)\,\mathrm{d}\Gamma$$

Moreover, the positive part of a function defines a monotone operator, that is

$$([g(u)]^+ - [g(v)]^+)([g(u)]^+ - [g(v)]^+) \leqslant ([g(u)]^+ - [g(v)]^+)(g(u) - g(v))$$

Hence, the lemma is satisfied with $C = (\min\{\alpha, 1\})^{-1}$.

On the other hand, taking $v = v_h$ in Equation (13) and using (14) we obtain

$$A(u_\varepsilon, v_h) - A(u_{\varepsilon h}, v_h) = 0, \quad \forall v_h \in \mathbf{V}_h \tag{15}$$

Now let us define the global error estimator η^* and the local error estimator η^*_T by

$$\eta^* = \left\{ \sum_{T \in \mathscr{T}_h} (\eta^*_T)^2 \right\}^{1/2} \tag{16}$$

$$\eta^*_T = \left\{ |T| \int_T R^2\,\mathrm{d}\Omega + \frac{1}{2} \sum_{\ell \in E_T} |\ell| \int_\ell (J^*_\ell)^2\,\mathrm{d}\Gamma \right\}^{1/2} \tag{17}$$

where

$$R = b + \mathrm{div}(\mathbf{T}(u_{\varepsilon h})) \quad \text{in } T, \ \forall T \in \mathscr{T}_h \tag{18}$$

is the residual of the local equilibrium equation at element level $T \in \mathscr{T}_h$ and

$$J_\ell^* = \begin{cases} [\![\mathbf{T}(u_{\varepsilon h})n]\!] & \forall \ell \in \mathscr{E}_\mathrm{I} \\ 0 & \forall \ell \subset \Gamma_u \\ 2(f - \mathbf{T}(u_{\varepsilon h})n) & \forall \ell \subset \Gamma_f \\ -2\{(\sigma_n(u_{\varepsilon h}) + \varepsilon^{-1}[g(u_{\varepsilon h})]^+)n + (\sigma_\tau(u_{\varepsilon h}))\tau\} & \forall \ell \subset \Gamma_c \end{cases} \tag{19}$$

is the residual of the equilibrium equation at element boundaries.

Lemma 2. For all $w \in \mathbf{V}$ we have

$$A(u_\varepsilon, w) - A(u_{\varepsilon h}, w) = \sum_T \left\{ (R, w)_T + \frac{1}{2} \sum_{\ell \in E_T} \langle J_\ell, w \rangle_\ell \right\}$$

where

$$(R, w)_T = \int_{\Omega_T} R \cdot w \, \mathrm{d}\Omega$$

$$\langle J_\ell, w \rangle_\ell = \int_{\Gamma_\ell} J_\ell \cdot w \, \mathrm{d}\Gamma$$

Proof. From the definition of $A(\cdot, \cdot)$ and from (13) and (14) it follows that

$$A(u_\varepsilon, w) - A(u_{\varepsilon h}, w) = l(w) - a(u_{\varepsilon h}, w) - \langle \varepsilon^{-1}[g(u_{\varepsilon h})]^+, g(w) \rangle$$

After integration by parts, the above expression can be rewritten as

$$\begin{aligned} A(u_\varepsilon, w) - A(u_{\varepsilon h}, w) &= \sum_T \left\{ (R, w)_T - \int_{\partial T} \mathbf{T}(u_{\varepsilon h})n \cdot w \, \mathrm{d}\Gamma \right\} + \int_{\Gamma_f} f w \, \mathrm{d}\Gamma - \langle \varepsilon^{-1}[g(u_{\varepsilon h})]^+, g(w) \rangle \\ &= \sum_T \left\{ (R, w)_T + \frac{1}{2} \sum_{\ell \in E_T} \langle J_\ell, w \rangle_\ell \right\} \end{aligned}$$

Then, from Lemmas 1 and 2 and Equation (15) we obtain

$$\begin{aligned} |e|_{1,\Omega}^2 + \|\varepsilon^{-1/2}([g(u_\varepsilon)]^+ - [g(u_{\varepsilon h})]^+)\|_{0,\Gamma_c}^2 &\leqslant C(A(u_\varepsilon, e) - A(u_{\varepsilon h}, e)) \\ &= C(A(u_\varepsilon, e - v_h) - A(u_{\varepsilon h}, e - v_h)) \\ &= C \sum_T \left\{ (R, e - v_h)_T + \frac{1}{2} \sum_{\ell \in E_T} \langle J_\ell, e - v_h \rangle_\ell \right\} \end{aligned} \tag{20}$$

Now, let us take the Clément interpolation of e which will be denoted by e^{I}. Hence, the following estimations are verified (see Reference [20])

$$\|e - e^{\mathrm{I}}\|_{0,T} \leqslant C|T|^{1/2}|e|_{1,\tilde{T}}$$

$$\|e - e^{\mathrm{I}}\|_{0,\ell} \leqslant C|\ell|^{1/2}|e|_{1,\tilde{T}}$$

where $\tilde{T}$ is the union of all the elements sharing a vertex with T. From these properties and Equation (20) we finally obtain

$$|e|_{1,\Omega}^2 + \|\varepsilon^{-1/2}([g(u_\varepsilon)]^+ - [g(u_{\varepsilon h})]^+)\|_{0,\Gamma_c}^2 \leqslant C\left\{\sum_T (|T|\|R\|_{0,T}^2 + \frac{1}{2}\sum_{\ell\in E_T}|\ell|\|J_\ell\|_{0,\ell}^2)\right\}^{1/2}|e|_{1,\Omega}$$

$$\leqslant C\left\{\sum_T \eta_T^2\right\}^{1/2}|e|_{1,\Omega} = C\eta^*|e|_{1,\Omega}$$

This expression provides the proof of the following theorem.

Theorem 1. There exists $C>0$ such that the global estimator η^* satisfies

$$|u_\varepsilon - u_{\varepsilon h}|_{1,\Omega} \leqslant C\eta^*$$

$$\|\varepsilon^{-1/2}([g(u_\varepsilon)]^+ - [g(u_{\varepsilon h})]^+)\|_{0,\Gamma_c} \leqslant C\eta^*$$

4. NUMERICAL TESTS WITH THE PENALIZED FORMULATION

In this section, we will perform adaptive analysis in several contact problems using the estimator η^* (Equation (16)). More specifically, due to the fact that the solution $u_{\varepsilon h}$ of (12) and the penetration term $\varepsilon^{-1}[g(u_{\varepsilon h})]$ are polluted with numerical error when ε is small, we use for $u_{\varepsilon h}$ the solution $u_{\varepsilon^k h}$ and for $\varepsilon^{-1}[g(u_{\varepsilon h})]$ the solution $\lambda_{\varepsilon^k h}$ (which plays the role of the force exerted by the foundation $\mathscr{F}$ on $\mathscr{B}$ across Γ_c) obtained by the augmented-Lagrangian method described in the Appendix (see also References [15, 17, 19]). In the following examples, we adopted $\varepsilon^{k+1} = 2/3\varepsilon^k$ and $\gamma = 10^{-8}$ for the residual of the complementarity relation between $\lambda_{\varepsilon^k h}$ and the gap $[g(u_{\varepsilon^k h})]$.

The numerical performance of the proposed estimator and its comparison with others in the literature will now be considered. Within the context of an adaptive procedure, an error estimator will be deemed efficient if the sequence of adaptive meshes produces an optimal reduction rate of the estimated error.

In addition to the previously introduced global estimator η^* (Equation (16)) we will also consider another alternative, even though not originally proposed for unilateral problems, the

Babuška–Miller estimator [5] η^{BM}

$$\eta^{\mathrm{BM}} = \left\{ \sum_{T \in \mathscr{T}_h} \left(\eta_T^{\mathrm{BM}}\right)^2 \right\}^{1/2} \tag{21}$$

$$\eta_T^{\mathrm{BM}} = \left\{ |T| \int_T R^2 \, \mathrm{d}\Omega + \frac{1}{2} \sum_{\ell \in E_T} |\ell| \int_\ell \left(J_\ell^{\mathrm{BM}}\right)^2 \mathrm{d}\Gamma \right\}^{1/2} \tag{22}$$

where

$$R = b + \mathrm{div}(\mathbf{T}(u_{\varepsilon h})) \quad \text{in } T, \ \forall T \in \mathscr{T}_h \tag{23}$$

is the residual of the local equilibrium equation at element level $T \in \mathscr{T}_h$ and

$$J_\ell^{\mathrm{BM}} = \begin{cases} [\![\mathbf{T}(u_{\varepsilon h})n]\!] & \forall \ell \in \mathscr{E}_{\mathrm{I}} \\ 0 & \forall \ell \subset \Gamma_u \\ 2(f - \mathbf{T}(u_{\varepsilon h})n) & \forall \ell \subset \Gamma_f \\ 0 & \forall \ell \subset \Gamma_c \end{cases} \tag{24}$$

To our knowledge, no error estimator for the Signorini problem is available for comparison. Notice that η^{BM} corresponds to our estimator η^* if the contribution of the contact boundary is neglected (i.e. treated as a Dirichlet boundary).

Let us now introduce a variant of our estimator as a consequence of the following consideration. The expression of J_ℓ^* along Γ_c is (see Equation (19))

$$J_\ell^* = 2((\sigma_n(u_{\varepsilon h}) + \varepsilon^{-1}[g(u_{\varepsilon h})]^+)n + \sigma_\tau(u_{\varepsilon h})\tau)$$

which can be rewritten as

$$J_\ell^* = 2(([\sigma_n(u_{\varepsilon h})]^+ - [\sigma_n(u_{\varepsilon h})]^- + \varepsilon^{-1}[g(u_{\varepsilon h})]^+)n + \sigma_\tau(u_{\varepsilon h})\tau) \tag{25}$$

where

$$[\sigma_n(u_{\varepsilon h})]^- = -\min\{0, \sigma_n(u_{\varepsilon h})\}$$

The tangential component $\sigma_\tau(u_{\varepsilon h})\tau$ is clearly identified with a spurious friction which is an evidence of local error because our problem is frictionless. On the other hand, a positive value (traction) in the normal component, given by $[\sigma_n(u_{\varepsilon h})]^+ n$, is also an evidence of local error because we have an unilateral contact problem, i.e. traction forces are not allowed along the contact boundary Γ_c. On the other hand, when $\sigma_n(u_{\varepsilon h})$ is negative some cancellation will occur with the penetration term $\varepsilon^{-1}[g(u_{\varepsilon h})]^+$ (which plays the role of a reaction force). However, due to the fact that the solution $u_{\varepsilon h}$ of (12) and the penetration term $\varepsilon^{-1}[g(u_{\varepsilon h})]$ are polluted with numerical error when ε is small, this cancellation is unlikely to occur. As mentioned in the beginning of this section, this was the reason to use for $u_{\varepsilon h}$ the solution $u_{\varepsilon^k h}$ and for $\varepsilon^{-1}[g(u_{\varepsilon h})]^+$ the solution $\lambda_{\varepsilon^k h}$ obtained by the augmented-Lagrangian method.

The considerations above enable us to provide, as an alternative to η^*, the following estimator: η^{**} identical to η^* with J_ℓ^* along Γ_c defined now by J_ℓ^{**}

$$J_\ell^{**} = 2\left([\sigma_n(u_{\varepsilon^k h})]^+ n + \sigma_\tau(u_{\varepsilon^k h})\tau\right) \tag{26}$$

It should be noted that these three error estimators (η^*, η^{**} and η^{BM}) only differ in the term J_ℓ associated to the contact boundary (Equations (19), (24) and (26)). The η^* global error estimator proposed in this work contains all the terms that contribute to the error. The modified estimator η^{**} only contains some of the previous terms (they are the terms identified with spurious friction forces in a model which is frictionless, and spurious traction forces in a surface which only admit compression forces) while in the Babuška–Miller estimator, all these terms are neglegted. Therefore, for a given finite element mesh, the value of the estimated error obtained with the η^* estimator is bigger than the value obtained with the η^{BM} estimator. In turn, the value obtained with the η^{**} will be between the other ones two.

The numerical examples presented in this section (in particular, see Example 3, Figures 18, 20 and 22) corroborate the above-mentioned. Therefore, in an adaptive analysis we will hope that using the η^*-estimator the elements in the contact region should be smaller than the elements obtained with the η^{BM}-estimator (see Example 3). Despite the formal differences among these estimators, it is important to note that during the adaptive process, the contribution of J_ℓ^* in the global error spreads quickly to zero. Then in the limit (from the computational point of view the second or third adaptive iteration) the final behaviour of these three estimators should be similar.

It is necessary to point out that our estimator can be modified in order to be applied in more efficient methods to solve the contact problem. As an example, we can mention how to make this modification for the constraint function method [21, 22]. In this case it is enough to replace the contact force λ with the equivalent force $\varepsilon/g(u)$. Nevertheless, we decide to work with the direct penalization because it corresponds to a stronger nonlinearity.

4.1. Adaptive procedure

The adaptive procedure we perform is the same regardless of the specific estimator considered. Given an initial mesh $\mathscr{T}_0$, consisting of N_0 elements, we will successively refine the mesh, generating new meshes $\mathscr{T}_1$, $\mathscr{T}_2$, etc., with numbers of elements approximately given by $N_1 = 4N_0$, $N_2 = 4N_1$, etc. Each one of these meshes is generated using the *advancing front technique* [19, 23–28] trying to produce a uniform distribution of the local error estimator over all elements [29].

The error estimators are used to define the *relative* desired element size at each element T in the old mesh according to

$$h_{\mathrm{new}}^T = \frac{C}{\eta_T} h_{\mathrm{old}}^T \tag{27}$$

where h_{new}^T is the diameter of the elements in the new mesh at the location of the triangle T in the old mesh, which has diameter h_{old}^T and yields a local error estimator η_T. The normalization constant C is the expected local error indicator equally distributed over all elements in the new mesh

$$C = N^{-1/2}\eta \tag{28}$$

where η is one of the considered error estimators and N is the desired number of elements in the new mesh.

As mentioned before, our remeshing algorithm is based on the *advancing front technique*. In this technique, the mesh generator tries to build equilateral triangles in the metric defined by the variable metric tensor $\mathbf{S}$ which, at point X of the actual (old) mesh, takes the value defined by

$$\mathbf{S}(X) = \frac{1}{h(X)}\mathbf{I} \tag{29}$$

where $\mathbf{I}$ is the identity second-order tensor in the plane, $h_{\text{new}}(X)$ is the *diameter* of an element to be generated at point X and dynamically defined along the mesh adaptation process described below.

4.1.1. η-adaptive procedure.

1. For each element compute the local error η_T and the global error η.
2. Given a number of elements N in the new adapted mesh, the expected local error indicator, equally distributed on all elements in the new triangulation is given by (28).
3. The element size at element level T in the *old* mesh is estimated using expression (27).
4. From the information at element level, different approaches [3] can be chosen to find the distribution at finite element nodal level $h_{\text{new}}(P)$.
5. In the remeshing algorithm it has been assumed that all triangles in the new mesh will be equilateral; as this will never happen, the new mesh will only approximately consist of the desired number of elements. To force the equality between these two numbers, the element size h at nodal level, must be scaled. In particular, for the $h_{\text{new}}(P)$ distribution the expected number of elements in the new finite element mesh is given by

$$N_{\text{el}_{\text{new}}} = \frac{4}{\sqrt{3}} \int_{\Omega} \frac{1}{h^2}\, \mathrm{d}\Omega \tag{30}$$

6. Then, the scaled value for the element size at nodal level P is given by

$$h_{\text{new}}(P) \leftarrow \sqrt{\frac{N_{\text{el}_{\text{new}}}}{N}} \times h_{\text{new}}(P) \tag{31}$$

7. Generate the new mesh and return to the step 1.

4.2. Examples

For all the examples presented in this section the following analyses have been performed.

1. Stress analysis for meshes with quasi-unifom element size h, $h/2$, $h/4$ and $h/8$, (sometimes also $h/16$).
2. For the coarse and the most refined uniform mesh, the domain distribution of the error estimator η^* (denoted by EtaT in the figures) is presented.
3. Using the estimator η^* and the adaptive process described before, a 3 or 4-level adaptive analysis is performed. The first adapted mesh is obtained applying the adaptive procedure to the first coarse mesh taking the same number of elements. As mentioned, the automatic mesh generator [27] used in this work is based on the *advancing front technique* and cannot

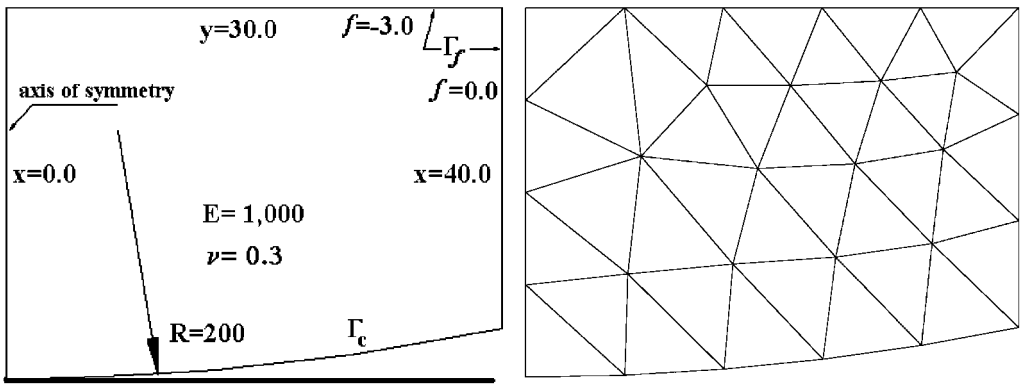

Figure 1. Problem 1. Data and first uniform mesh.

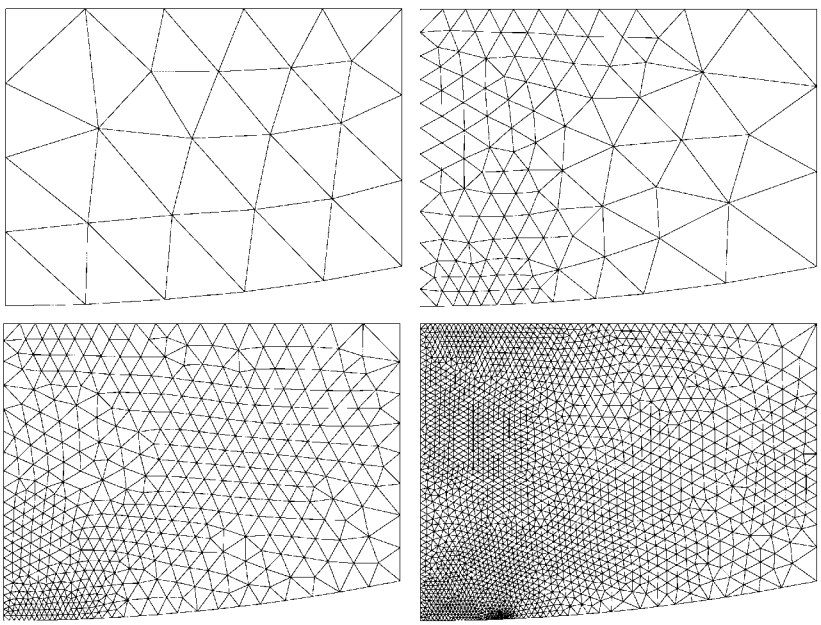

Figure 2. Problem 1. Adapted meshes.

control exactly the number of elements to be generated. Hence, the first adapted mesh has roughly the same number of elements as the coarse mesh has. The associated finite element meshes are presented together with the domain distribution of the error estimator η^* (denoted by EtaT in the figures).

4. The reduction rate for each estimator as a function of the number of nodes of the associated mesh, is also presented using log(error estimator) vs log(number of nodes) figures. In these figures, only the estimators η^* and η^{BM} are plotted, since the associated values for the η^{**} estimator are practically identical to η^{BM}. Also the notation 'um' and 'am' are used for

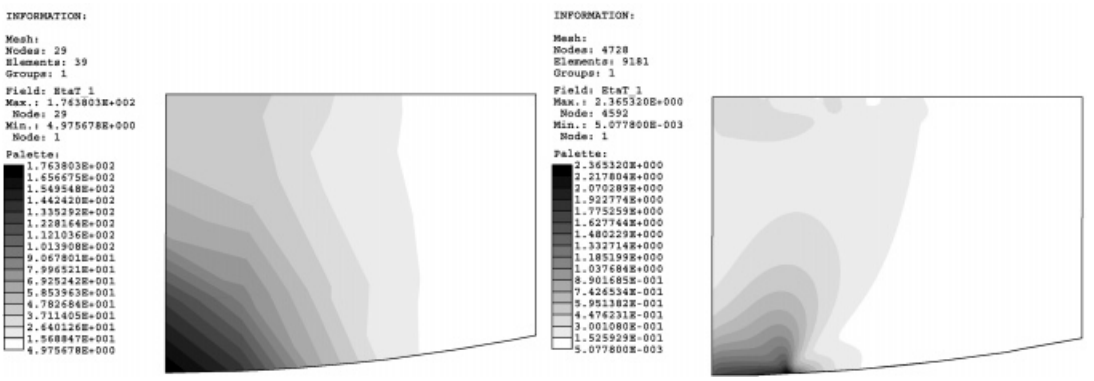

Figure 3. Problem 1. η^* error distribution for the coarse and the most refined uniform meshes.

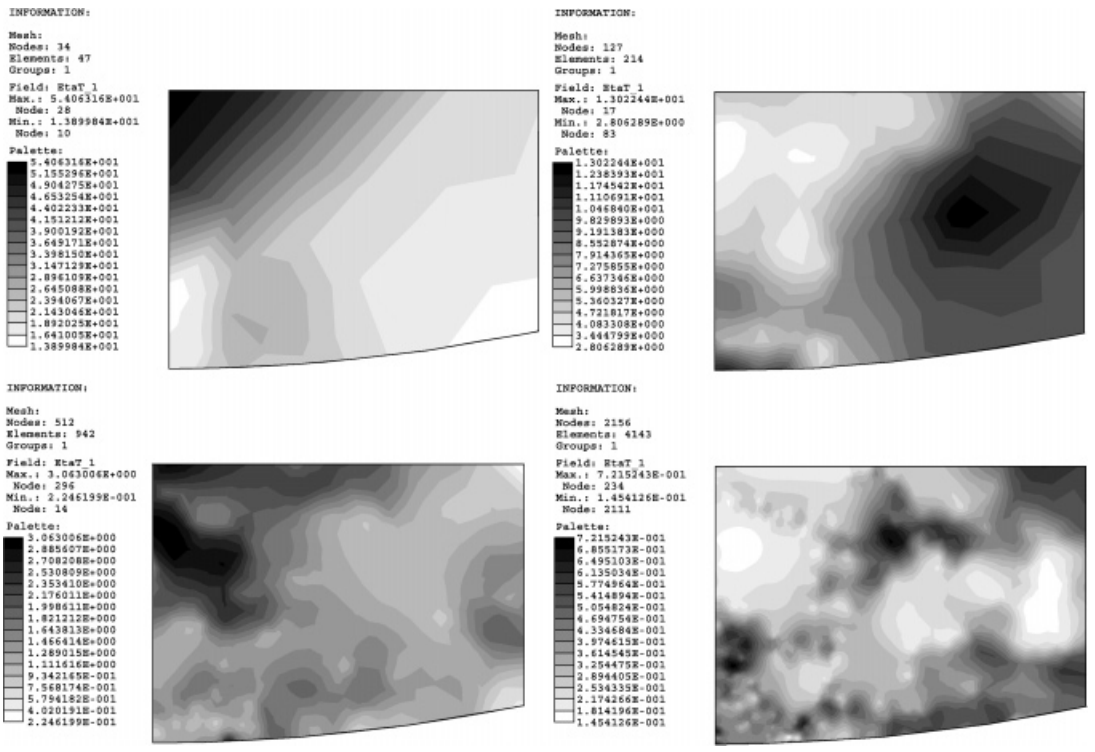

Figure 4. Problem 1. η^* error distribution for η^*-adaptive procedure.

results obtained with **u**niform and **a**dapted **m**eshes. In the same figures, the maximum values of the estimator η^*, denoted by ${}^{\max}\eta^*$, are also plotted for uniform and adapted meshes, respectively.

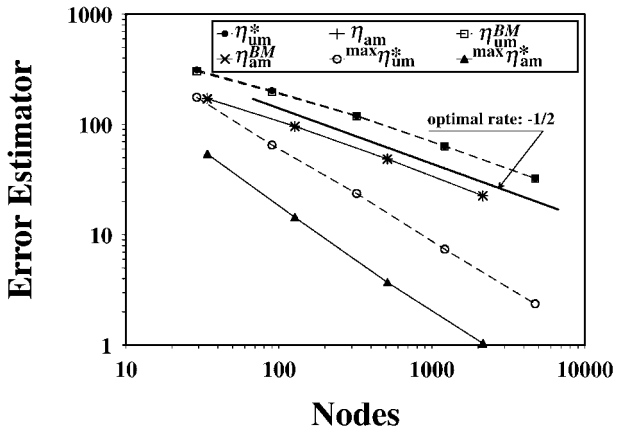

Figure 5. Problem 1. Reduction rate of the error estimator η^* and η^{BM}.

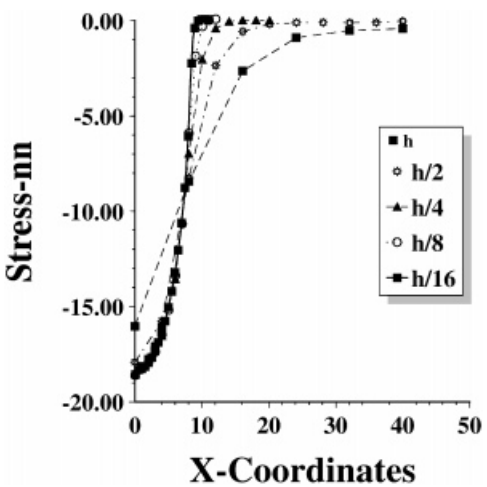

Figure 6. Problem 1. Contact reaction evolution for uniform meshes.

Problem 1. The first example is a plane stress problem with unilateral boundary conditions inducing a discontinuity on the contact reaction stresses distribution along the contact boundary Γ_c. The data of the problem are described in Figure 1 together with the first coarse uniform mesh which has 29 nodes and 39 elements. The *finest* uniform mesh ($h/16$) has 4728 nodes and 9181 elements. Figure 2 shows the sequence of meshes obtained with the adaptive procedure taking η^* as the error estimator (34 nodes and 47 elements for the first, 127 nodes and 214 elements for the second, 512 nodes and 942 elements for the third and 2156 nodes and 4143 elements for the most refined adapted mesh). As mentioned, the first adapted mesh is obtained applying the adaptive procedure on the first coarse mesh and taking the same number of elements for the two meshes. The distribution of the error estimator for uniform and adaptive refinements are shown in Figures 3 and 4, respectively. Since no singularities are found in this problem, the adaptive procedure

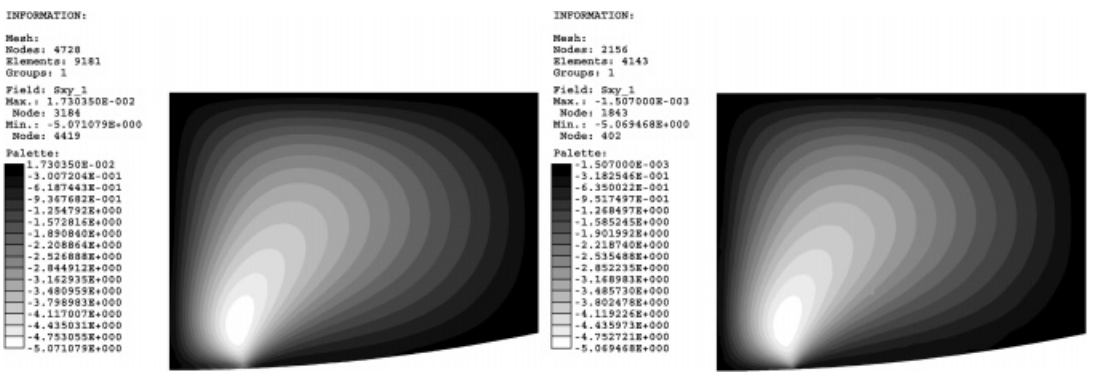

Figure 7. Problem 1. $\mathbf{T}_{xy}$ stress distribution for the most refined uniform mesh ($h/16$) and the last adapted mesh.

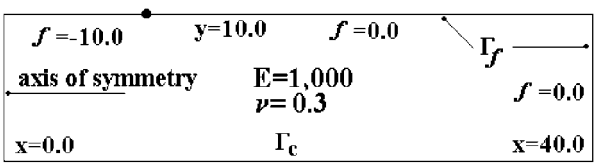

Figure 8. Problem 2. Data.

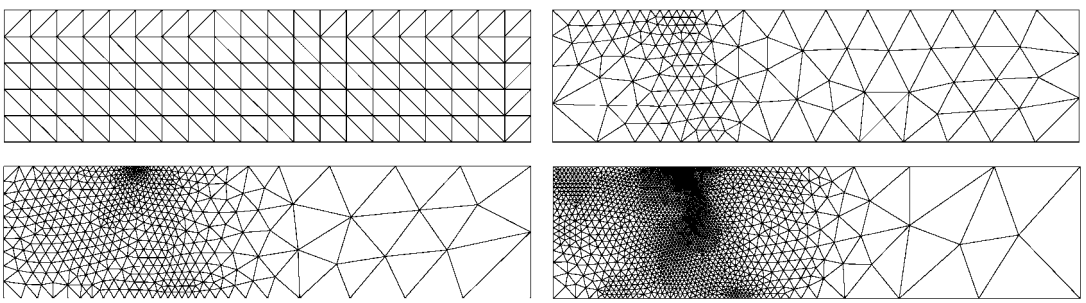

Figure 9. Problem 2. First uniform mesh and adapted meshes.

and the sequence of uniform meshes produce an optimal reduction rate of the error estimator. The performance of the different error estimators are presented in Figure 5. The derivative of the contact reaction along the boundary has a point of discontinuity (see Figure 6). As expected, this discontinuity produces a concentration of elements in the neighbourhood of this point during the adaptive process. Moreover, this point of discontinuity is clearly depicted by the distribution of the stress $\mathbf{T}_{xy}$. Figure 7 shows this distribution for the most refined uniform (4728 nodes) and adapted (2156 nodes) meshes, respectively.

Problem 2. The second example is again a plane stress problem but now the discontinuity is induced by the distribution of applied loads on Γ_f and (less severe) by the contact reaction distribution. The data of the problem are shown in Figure 8. The first coarse uniform mesh,

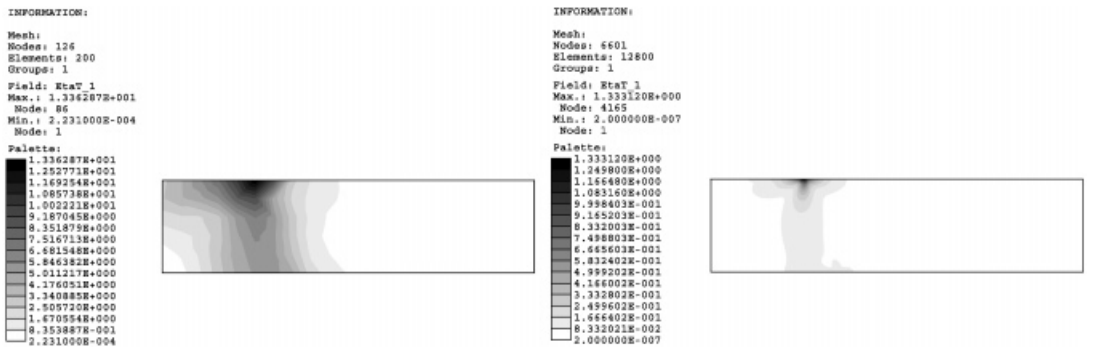

Figure 10. Problem 2. η^* error distribution for the coarse and the most refined uniform mesh.

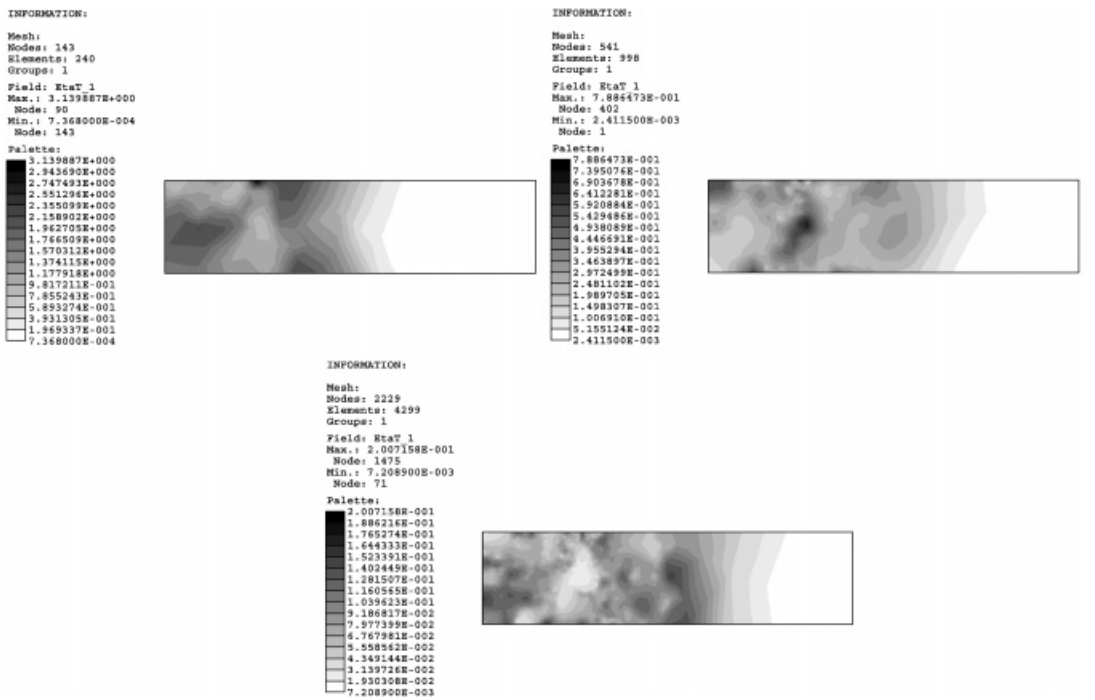

Figure 11. Problem 2. η^* error distribution for η^*-adaptive procedure.

with 126 nodes and 200 elements, is shown in Figure 9. The most refined mesh ($h/8$) has 6601 nodes and 12 800 elements. Figure 9 also shows the sequence of meshes obtained with the adaptive procedure taking η^* as the error estimator (the first mesh has 143 nodes and 240 elements, the second has 541 nodes and 998 elements and the third has 2229 nodes and 4299 elements). The distribution of the error estimators for uniform refinement and the η^*-adaptive procedure are shown in Figures 10 and 11, respectively. Since no strong singularities occur in this problem, the adaptive procedure and the sequence of uniform meshes produce an optimal reduction rate

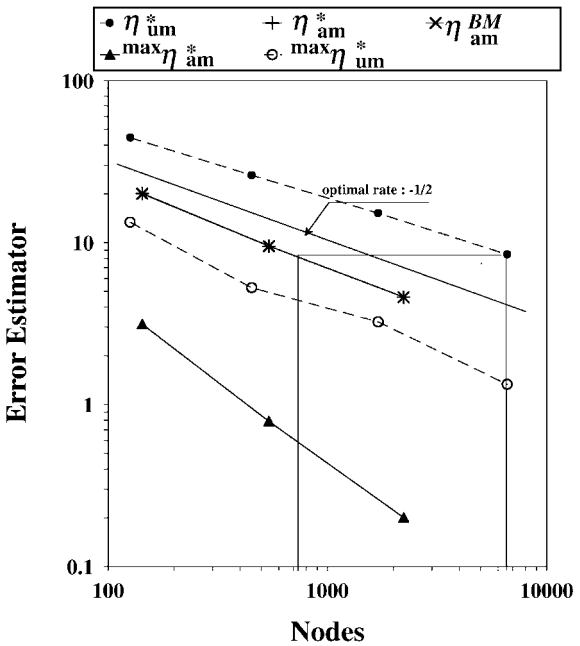

Figure 12. Problem 2. Reduction rate of the error estimator η^* and η^{BM}.

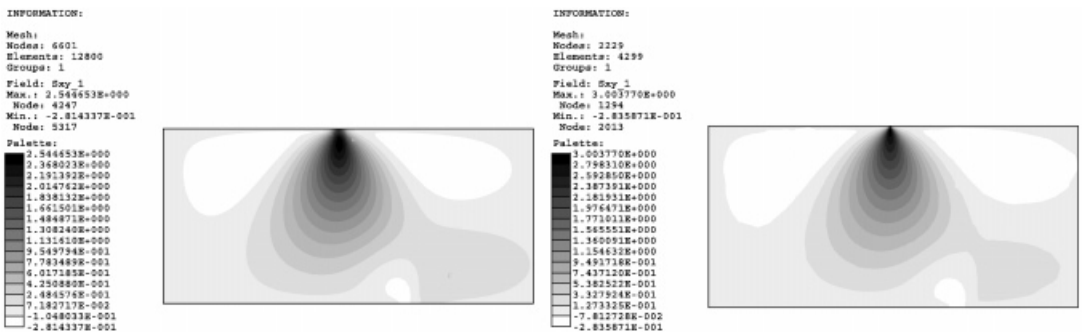

Figure 13. Problem 2. $\mathbf{T}_{xy}$ stress distribution for the most refined uniform mesh ($h/8$) and the last adapted mesh.

of the error estimator. The performances of the different error estimators are presented in Figure 12. The two points of discontinuity are clearly detected by the distribution of the stress $\mathbf{T}_{xy}$. Figure 13 shows this distribution for the most refined uniform mesh (6601 nodes) and for the last adapted mesh (2229 nodes), respectively. As expected, these discontinuities produce a concentration of elements in the neighbourhood of these points. Finally, Figure 14 shows the evolution of the contact reaction for the sequence of uniform meshes.

Problem 3. The third example is a continuous beam, modeled as a plane stress problem, under the action of a uniform vertical load and with discontinuous rigid unilateral contact support inducing

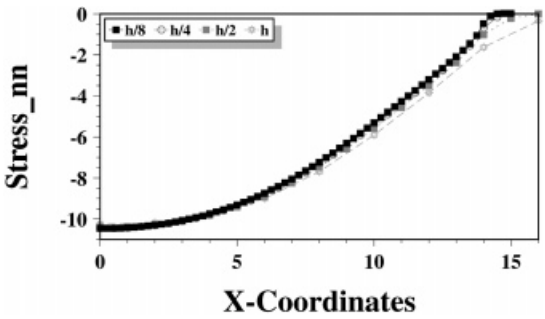

Figure 14. Problem 2. Contact reaction evolution for uniform meshes.

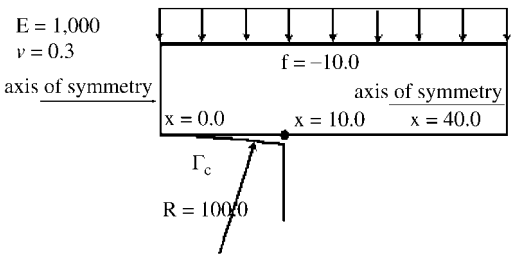

Figure 15. Problem 3. Data.

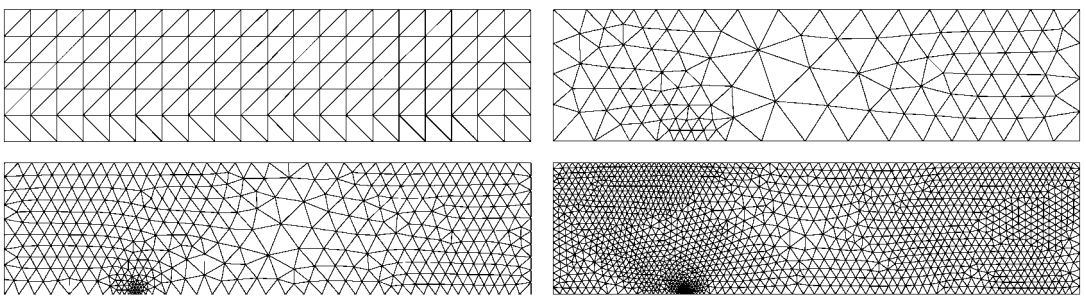

Figure 16. Problem 3. First uniform mesh and adapted meshes.

a strong singularity. The data of the problem is shown in Figure 15. The first coarse uniform mesh which has 126 nodes and 200 elements is shown in Figure 16. The most refined mesh ($h/8$) has 6601 nodes and 12 800 elements. Figure 16 also shows the sequence of meshes obtained with the adaptive procedure taking η^* as the error estimator. The evolution of the error estimators for uniform refinement and the adaptive procedure are shown in Figures 17 and 18, respectively. Due to the singularity, a strong concentration of elements in the neighborhood of this point is obtained. Moreover, only the adaptive procedure produces an optimal reduction rate of the error estimator. The performances of the different error estimators are presented in Figure 19.

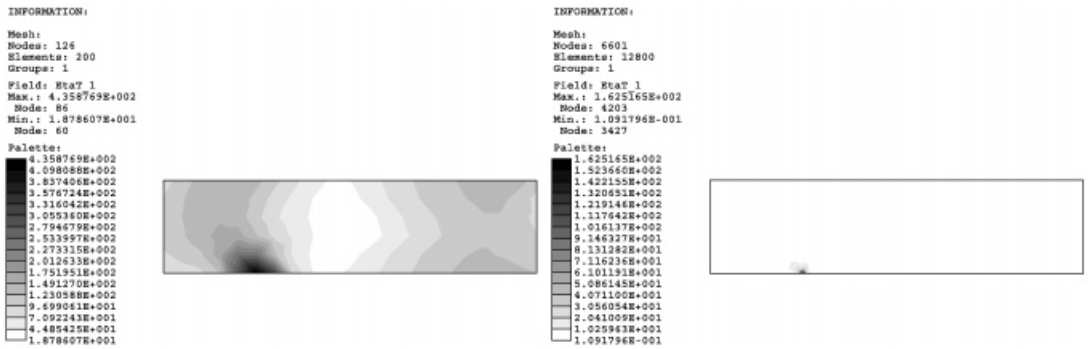

Figure 17. Problem 3. η^* error distribution for the coarse and the most refined uniform mesh.

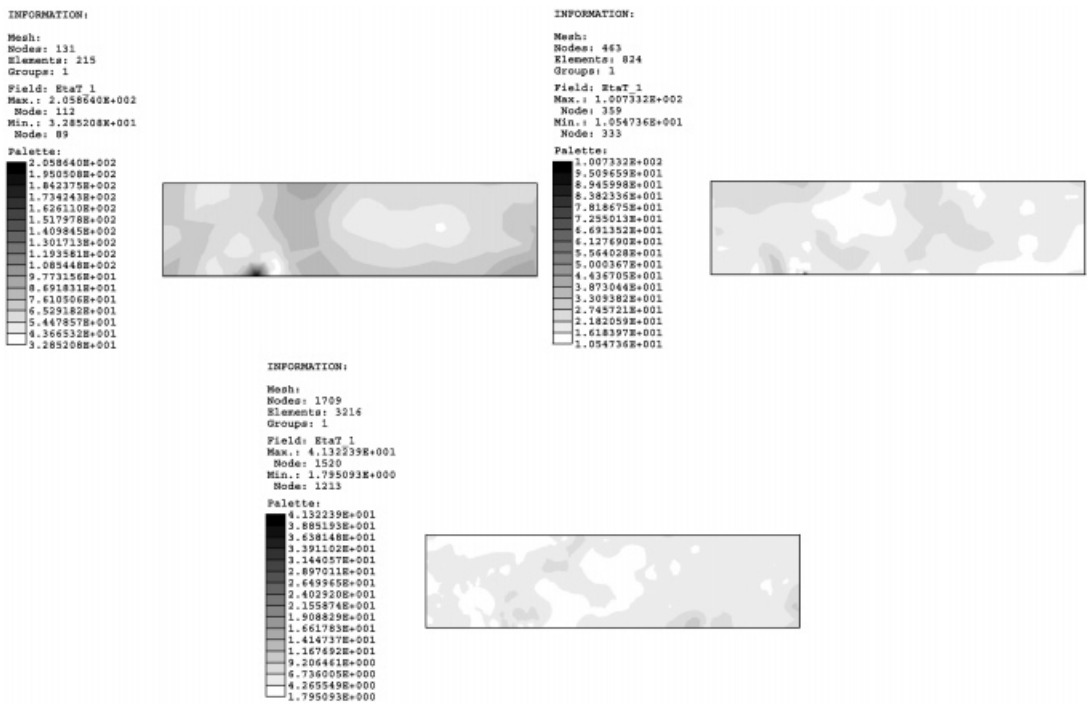

Figure 18. Problem 3. η^* error distribution for η^*-adaptive procedure.

Figure 20 shows the distribution of the Babuška–Miller estimator η^{BM} for the first adapted mesh, using η^*-adaptive procedure. This distribution is quite similar to the distribution of η^* shown in Figure 18. Its maximum value is approximately 30 per cent less than the maximum of the latter estimator. Hence, if we use an η^{BM}-adaptive procedure, the appearance of the finite element meshes will be qualitative similar to the ones obtained with an η^*-adaptive procedure. However, near the point of singularity, the element size will be greater as we can see in Figure 21, where the finite element meshes obtained with the Babuška–Miller estimator-adaptive procedure are shown.

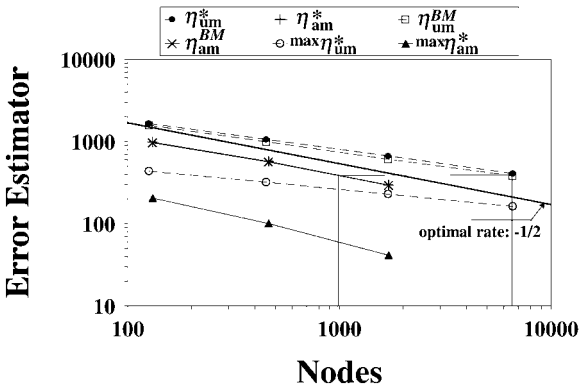

Figure 19. Problem 3. Reduction rate of the error estimator η^* and η^{BM}.

Figure 20. Problem 3. Distribution of the η^{BM} error estimator for the first adaptive mesh using the η^*-adaptive procedure.

Figure 22 shows the distribution of the η^* error estimator for each adapted finite element mesh obtained with the η^{BM}-adaptive procedure.

5. FINAL REMARKS

The proposed adaptive analysis for the contact problems studied in this work, induces a strong computational cost reduction. In fact, for Problem 1, Figure 7 shows that the adaptive strategy requires half of the nodes needed by uniform refinement to obtain the same results. For Problem 2, Figure 13 shows that the adaptive analysis requires only 1/3 of the nodes needed by

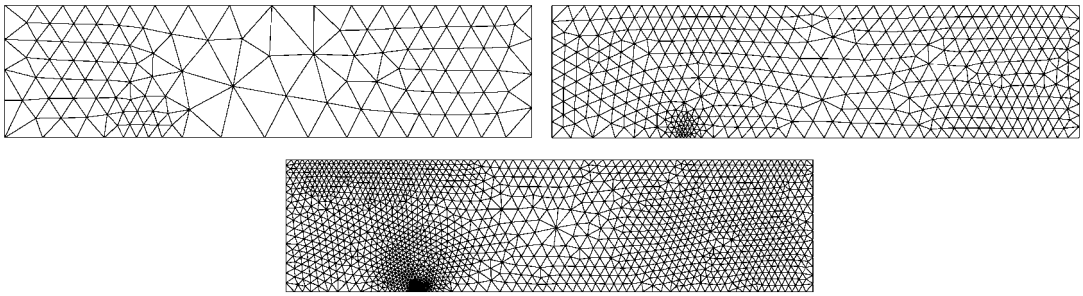

Figure 21. Problem 3. Adapted meshes for η^{BM}-adaptive procedure.

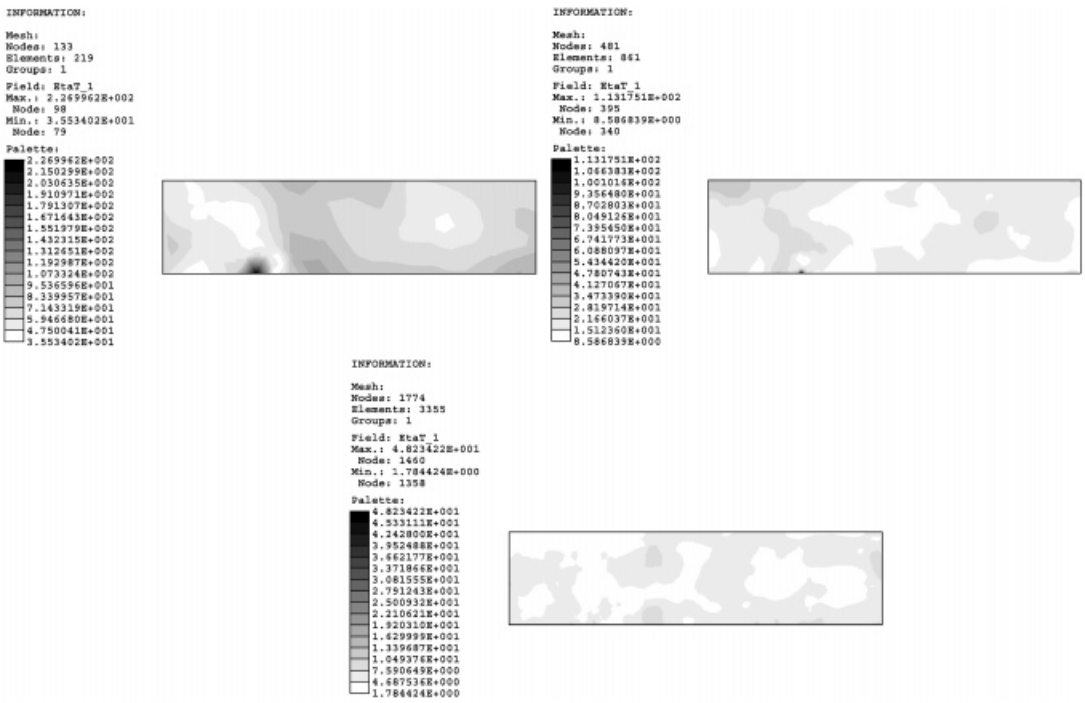

Figure 22. Problem 3. η^* error distribution for adapted meshes using an η^{BM}-adaptive procedure.

the other refinement technique. Moreover, using the proposed global error estimator as an indicator of the quality of the approximate solution, we observe that the adaptive strategy requires values ranging from 1/4 to 1/10 of the number of nodes when compared with the uniform refinement approach (see Figures 5, 12 and 19).

On the other hand, the numerical performance of the η^* error estimator confirms the theoretical results presented in Section 3. Moreover, let $\mathcal{N}$ be the number of nodes in the finite element mesh then, for singular contact problems, the optimal reduction rate $\mathcal{O}(\mathcal{N}^{-1/2})$ is also obtained using our η-adaptive procedure with η being any of the error estimators η^*, η^{**} or η^{BM}. Notice also

that using our adaptive procedure, the reduction rate associated with the maximum of the error indicator is of the type $\mathcal{O}(\mathcal{N}^{-1})$ (see Figures 5 and 12) and $\mathcal{O}(\mathcal{N}^{-1/2})$ for the third problem (see Figure 19).

The formal differences among these three error estimators (η^*, η^{**} and η^{BM}) are restricted to the contribution of the contact boundary into the total error estimator. For the η^{BM}-estimator, this contribution is zero, for the η^{**}-estimator this contribution is associated with friction and to the positive part of the normal surface traction. For the η^*-estimator, this contribution is associated with the friction surface traction and to the jump between internal and external (reaction) normal surface traction. Apparently, these contributions become negligible along the adaptive procedure, rendering all estimators approximately equivalent in what concerns mesh refinement specification.

From the above considerations any of these estimators can be used in contact problems. However, from a computational point of view, singularities (or discontinuities) are better detected using the η^*-adaptive procedure (see, for example, Figures 18 and 20).

APPENDIX A: THE AUGMENTED-LAGRANGIAN ALGORITHM

It is well known that penalty formulations have the drawback that numerical unstabilities arise for small values of ε, which in turn are needed to simulate the exact indicator function I_K. Moreover, within this approximation the complementary equation $\sigma_n(u_{\varepsilon h})g(u_{\varepsilon h})=0$ is not satisfied along Γ_c. To overcome this difficulty we use in this paper a penalty function that is the result of an augmented-Lagrangian formulation (see Reference [18])

$$0 \leqslant \lambda_{\varepsilon h} \leqslant C, \quad P_\varepsilon(u_{\varepsilon h}, \lambda_{\varepsilon h}) = \frac{\varepsilon}{2}\sum_{i\in I}\left\{\left[\max\left(0; \lambda_{\varepsilon h,i} + \frac{1}{\varepsilon}g(u_{\varepsilon h}(x_i))\right)\right]^2 - \lambda_{\varepsilon h,i}^2\right\} \tag{A1}$$

The algorithm consists in a sequence of k traditional penalization problems yielding equilibrated solutions $u_{\varepsilon^k h}$ for fixed values of $\lambda_{\varepsilon^k h}$ and ε^k. Then, the minimization procedure is

(0) Given $\lambda_{\varepsilon^0 h}$, $\varepsilon^0 > 0$, $k = 0$
(1) Find $u_{\varepsilon^k h} \in \mathbf{V}_h$

$$u_{\varepsilon^k h} = \arg \inf_{v\in\mathbf{V}_h}\{\tfrac{1}{2}a(v,v) - l(v) + P_\varepsilon(v, \lambda_{\varepsilon^k h})\}$$

(2) For $i \in I$ find

$$\lambda_{\varepsilon^{k+1}h,i} = \max\left\{0; \lambda_{\varepsilon^k h,i} + \frac{1}{\varepsilon}g(u_{\varepsilon^k h}(x_i))\right\}$$

(3) If $\lambda_{\varepsilon^{k+1}h,i}\, g(u_{\varepsilon^k h}(x_i)) \leqslant \gamma \ \forall i \in I$ STOP
Else: $\varepsilon^{k+1} < \varepsilon, k = k+1$, GOTO (1).

Step (1) is solved by the quasi-Newton technique and global convergence is achieved for an equilibrated configuration whose complementary equation (Step (3)) is (numerically) equal to zero. In the examples shown in this paper, we adopted $\varepsilon^{k+1} = 2/3\varepsilon^k$ and $\gamma = 10^{-8}$.

ACKNOWLEDGEMENTS

This work was partially supported by Conselho Nacional de Desenvolvimento Científico e Tecnológico (CNPq), Brazil, by Consejo Nacional de Investigaciones Científicas y Técnicas (CONICET), Argentina, and by Fundação de Amparo à Pesquisa do Estado de Rio de Janeiro (FAPERJ). The authors gratefully acknowledge the software facilities provided by the TACSOM Group (www.lncc.br/~tacsom).

REFERENCES

1. Ainsworth M, Oden JT, Lee CY. Local *a posteriori* error estimators for variational inequalities. *Numerical Methods for P. D. E.* 1993; **9**:23–33.
2. Johnson C. Adaptive finite element methods for the obstacle problem. *Mathematics Modelling and Methods in Applied Science* 1992; **2**(4):483–487.
3. Zienkiewicz OC, Taylor RL. *The Finite Element Method.* McGraw-Hill: New York, 1989.
4. Noor AK, Babŭska I. Quality assessment and control of finite element solutions. *Finite Elements in Analysis and Design* 1987; **3**:1–26.
5. Babuška I, Miller A. *A posteriori* error estimates and adaptive techniques for the finite element method. *Technical Note BN-968*, Institute for Physical Science and Technology. University of Maryland, 1981.
6. Babuška I, Miller, A. A feedback finite element method with *a posteriori* error estimation. Part I: The finite element method and some basic properties of the *a posteriori* error estimator. *Computer Methods in Applied Mechanics and Engineering*, 1987; **61**:1–40.
7. Babuška I, Rheinboldt WC. *A posteriori* error estimators in the finite element method. *International Journal for Numerical Methods in Engineering* 1978; **12**:1587–1615.
8. Bank RE, Weiser A. Some *a posteriori* error estimators for elliptic partial differential equations. *Mathematics of Computation* 1985; **44**:283–301.
9. Verfürth R. A posteriori error estimators for the Stokes equations. *Numerical Mathematics* 1989; **55**:309–325.
10. Hlaváček L, Haslinger J, Nečas J, Lovíšek J. *Solution of Variational Inequalities in Mechanics*, Series of Applied Mathematical Sciences, Vol. 66. Springer: New York, 1982.
11. Panagiotopoulos PD. *Inequality Problems in Mechanics and Applications. Convex and Nonconvex Energy Functions.* Birkhaüser: Basel, 1985.
12. Kikuchi N, Oden JT. *Contact Problems in Elasticity: A Study of Variational Inequalities and Finite Element Methods.* SIAM: Philadelphia, PA, 1988.
13. Glowinski R. *Numerical Methods for Nonlinear Variationals Problems*. Springer: Berlin, 1984.
14. Herskovits J. Interior point algorithms for nonlinear constrained optimization. In *Lecture notes of Optimization of Large Structural Systems* — NATO/DFG ASI, Rozvany G. (ed.). Essen University, Germany, 1991.
15. Fancello EA, Feijóo RA. Shape optimization in frictionless contact problems. *International Journal for Numerical Methods in Engineering* 1994; **37**:2311–2335.
16. Hevsukoff AG. Sobre a introdução de um algoritmo de ponto interior no ambiente de projeto de engenharia. *M.Sc. Thesis*, Federal University of Rio de Janeiro, Brazil, 1991.
17. Fancello EA, Haslinger J, Feijóo RA. Numerical comparison between two cost functions in contact shape optimization. *Structural Optimization* 1995; **9**:57–68.
18. Bertsekas DP. *Constrained Optimization and Lagrange Multiplier Methods*. Academic Press: New York, 1982.
19. Fancello EA. Análise de Sensibilidade, Geração Adaptativa de Malhas e o Método dos Elementos Finitos na Otimização de Forma em Problemas de Contato e Mecânica da Fratura. *D.Sc. These*, Federal University of Rio de Janeiro, Brazil, 1993.
20. Clément, P. Approximation by finite element function using local regularization. *RAIRO* 1975; **R-2**:77–84.
21. Bathe KJ. *Finite Elements Procedures*. Prentice-Hall: Englewood Cliffs, NJ, 1996.
22. Bathe KJ, Bouzinov PA. On the constraint function method for contact problems. *Computers and Structures* 1997; **64**:1069–1085.
23. Peiró J. A finite element procedure for the solution of the Euler equations on unstructured meshes. *Ph.D. Thesis*, Department of Civil Engineering, University of Swansea, UK, 1989.
24. Peraire J, Morgan K, Peiró J. Unstructured mesh methods for CFD. *I. C. Aero Report* no 90-04, Imperial College, UK, 1990.
25. Peraire J, Peiró J, Morgan K. Adaptive remeshing for three-dimensional compressible flow computations. *Journal of Computational Physics* 1992; **103**:269–285.
26. Peraire J, Peiró J, Morgan K, Zienkiewicz OC. Adaptative remeshing for compressible flow computations. *Journal of Computational Physics* 1987; **72**:449–466.
27. Fancello EA, Guimarães AC, Feijóo RA, Vénere MJ. 2D Automatic mesh generation by Object Oriented Programming. *Proceedings of the 11th Brazilian Congress of Mechanical Engineering of the Brazilian Association of Mechanical Sciences*, São Paulo, Brazil, 1991, pp. 635–638, in Portuguese.

28. de Oliveira M, Guimarães ACS, Feijóo RA, Vénere MJ, Dari EA. An object oriented tool for automatic surface mesh generation using the advancing front technique. *International Journal for Latin America Applied Research* 1997; **27**:39–49
29. Zienkiewicz OC, Zhu JZ. A simple error estimator and adaptive procedure for practical engineering analysis. *International Journal for Numerical Methods in Engineering* 1987; **24**:337–357.
30. Buscaglia GC, Feijóo RA, Padra C. *A posteriori* error estimation in sensitivity analysis. *Structural Optimization* 1995; **9**:194–199.
31. Ekeland I, Temam R. *Convex Analysis and Variational Problems*. North-Holland: Amsterdam and American Elsevier: New York, 1976.

